

The effect of momentum anisotropy on quark matter in the quark-meson model

He-Xia Zhang*

*Key Laboratory of Quark & Lepton Physics (MOE) and Institute of Particle Physics,
Central China Normal University, Wuhan 430079, China*

Ben-Wei Zhang†

*Key Laboratory of Quark & Lepton Physics (MOE) and Institute of Particle Physics,
Central China Normal University, Wuhan 430079, China and
Institute of Quantum Matter, South China Normal University, Guangzhou 510006, China*

We investigate the chiral phase structure of quark matter with spheroidal momentum-space anisotropy specified by one anisotropy parameter ξ in the 2+1 flavor quark-meson model. We find that the chiral phase diagram and the location of the critical endpoint (CEP) are affected significantly by the value of ξ . With the increase of ξ , the CEP is shifted to smaller temperatures and larger quark chemical potentials. And the temperature of the CEP is more sensitive to the anisotropy parameter than the corresponding quark chemical potential, which is opposite to the study for finite system volume effect. Furthermore, the effects of momentum anisotropy on the thermodynamic properties and scalar (pseudoscalar) meson masses are also studied at vanishing quark chemical potential. The numerical results show that an increase of ξ can hinder the restoration of chiral symmetry. We also find that shear viscosity and electrical conductivity decrease as ξ grows. However, bulk viscosity exhibits a significant non-trivial behavior with ξ in the entire temperature domain of interest.

I. INTRODUCTION

Quantum chromodynamics (QCD) is the fundamental theory for describing the strong interaction, and its phase structure is an important subject of great interest in recent decades. The first-principle results from lattice QCD simulation [1, 2] have indicated that with increasing temperature T , the transition from the ordinary nuclear matter to the chiral symmetric quark-gluon plasma (QGP) is a smooth crossover at small or zero chemical potential μ . At large chemical potential, lattice QCD simulation as a reliable tool to obtain the chiral properties of QCD matter, confronts a great challenge due to the fermion sign problem [3], although different strategies (for reviews see, e.g., Refs. [4–6]), such as Taylor series expansions [7–9], imaginary chemical potential, reweighting techniques [10, 11], complex Langevin method [12, 13], have been developed to try to tackle this problem. In this context, some alternative theoretical tools, such as QCD low-energy effective models (e.g. the Nambu-Jona-Lasinio model [14–16], Polyakov-loop extended NJL (PNJL) model [17–19], quark-meson model or linear sigma model [20–24], Polyakov quark-meson (PQM) model [25–28]), Dyson-Schwinger equation approach [29, 30], the functional renormalization group approach [31–34], which are not restricted by chemical potential, have been proposed to better explore the QCD phase structure at high chemical potential. And the results from the effective model calculations [35, 36] show that the chiral phase

transition of the strongly interacting matter is a first-order transition at high density, and a second-order critical endpoint (CEP) can exist between the crossover line and the first-order phase transition line in the (μ, T) -plane. Apart from the phase transition, other important informations, such as thermodynamic properties, in-medium properties of mesons [36, 37] and transport properties [38–40] for the strongly interacting matter are also extensively studied in these QCD effective models.

To take into account the intricacy of the realistic quark matter produced in relativistic heavy-ion collisions (HICs) at the RHIC and the LHC, different improved versions of the QCD effective models have been proposed by including the effects of the finite volume of the system [42–57], the non-extensive effects in term of long-distance correlation [58, 59], the presence of magnetic fields [60–69], and the effects of electric field [71–75], to better explore the chiral/confinement properties of the strongly interacting matter at finite temperature or quark chemical potential. Conventionally, in the literature, all the effective models or improved effective models are based on an ideal assumption that the constituents of quark matter are completely isotropic in momentum-space for the absence of magnetic fields. However, due to the geometry of fireball created in HICs is asymmetric, the system evolves with different pressure gradients along different directions. As a result, the expanding and cooling rate along the beam direction (denotes as longitudinal direction) is larger than radial direction [76] and this momentum anisotropy can survive in all the stages of the HICs, consequently, the parton-level momentum distribution functions may become anisotropic. Thus, it's essential to consider the momentum-space anisotropy induced by the rapid longitudinal asymptotic expansion into the

* hexiazhang@mails.ccnu.edu.cn

† bwzhang@mail.ccnu.edu.cn

phenomenological investigation of different observables. Up to present, extensive works have been made to explore the effects of momentum anisotropy on the parton self-energy [76–79], photon and dilepton production [80–83], the dissociation of quarkonium [84–86], heavy-quark potential [87, 88], various transport coefficients [89–92], jet quenching parameter [93] which, are sensitive to the evolution of the QGP. And associated results have indicated that the momentum-space anisotropy has a significant effect on the observables of the QGP. However, with the best of our knowledge, so far there is no study of momentum anisotropy in the framework of effective QCD models and no research regarding the effect of momentum-space anisotropy on chiral phase transition. Inspired by this fact, one major goal of present work is to reveal how the momentum anisotropy qualitatively affects the chiral phase structure as well as transport properties in the strongly interacting matter.

The present paper is a first attempt to study the effect of the momentum-space anisotropy induced by the rapid longitudinal expansion of fireball created in HICs on the QCD chiral phase transition. We adopt the 2+1 flavor quark-meson model, which is successful in describing the mechanism of spontaneous chiral symmetry breaking, to approximate quark matter. The effect of momentum anisotropy enters in the quark-meson model by substituting the isotropic (local equilibrium) distribution function in the total thermodynamical potential with the anisotropic one. This introduces one more degree of freedom, *viz.*, the direction of anisotropy. The anisotropic parameter ξ , representing the degree of momentum anisotropy or the tendency of the system to stay away from the isotropic state, is also considered as argument into the isotropic distribution function. Based on this momentum anisotropy-dependent quark-meson model, we first explore how the momentum anisotropy affects the chiral phase diagram and the location of CEP. Next, we investigate the thermodynamic properties and the thermal properties of various scalar (pseudoscalar) meson masses for vanishing chemical potential in both isotropic and anisotropic quark matter. Finally, transport coefficients, such as shear viscosity, electrical conductivity, and bulk viscosity, which are crucial to understand the dynamical evolution of QCD matter, also are estimated in an (an-)isotropic quark matter. Note that we restrict ourselves here to the anisotropic system close to isotropic local equilibrium state, consequently, the calculations of thermodynamic quantities, meson masses and transport coefficients in the anisotropic system are methodologically similar to those in the isotropic system. Especially, in the small ξ limit, the anisotropic distribution can just linearly expand to the linear order of ξ . Using this linear approximation of the anisotropic distribution, the mathematical expression of transport coefficients, which are obtained by solving the relativistic Boltzmann equation under the relaxation time approximation, can be explicitly separated into an equilibrium part and an anisotropic correction part [89–

92]. For $\xi \rightarrow 0$, the analytic expressions can reduce to the standard expressions in the local equilibrium medium, which can be seen in Section. IV.

This paper is organized as follows. In section. II, we give a brief overview of the three-flavor quark-meson model. In section. III, the modification of the thermodynamical potential within momentum-space anisotropy is presented. In section. IV, we discuss the chiral phase transition, thermodynamics properties, meson masses, and transport coefficients in both isotropic and anisotropic quark matter. In section. V, we summarize the main results and give an outlook.

II. THE QUARK-MESON MODEL

The quark-meson model as a successful QCD-like effective model can capture an important feature of QCD, namely, chiral symmetry breaking and restoration at high temperature/density. The Lagrangian of the three-flavor quark-meson model presently used for our purpose is taken from Ref. [23]:

$$\mathcal{L}_{\text{QM}} = \bar{\Psi}(i\gamma_\mu D^\mu - g\phi_5)\Psi + \mathcal{L}_{\text{M}}, \quad (1)$$

where $\Psi = u, d, s$ stands for the quark field with three flavors ($N_f = 3$) and three color degrees of freedom ($N_c = 3$). The first term in the right hand side of Eq. (1) represents the interaction between the quark field and the scalar (σ) and pseudoscalar (π) fields with a flavor-blind Yukawa coupling g of the quarks to the mesons. The meson matrix is given as

$$\phi_5 = T_a(\sigma_a + i\gamma_5\pi_a), \quad (2)$$

where $T_a = \lambda_a/2$ with $a = 0, \dots, 8$ are the nine generators of the $U(3)$ symmetry. λ_a is Gell-Mann matrix with $\lambda_0 = \sqrt{\frac{2}{3}}1$. σ_a and π_a denote the scalar meson nonet and the pseudoscalar meson nonet, respectively.

The second term in Eq. (1) is the purely mesonic contribution, \mathcal{L}_{M} , which describes the chiral symmetry breaking pattern in strong interaction. It is given by [23]

$$\begin{aligned} \mathcal{L}_{\text{M}} = & \text{Tr}(\partial_\mu \phi^\dagger \partial^\mu \phi - m^2 \phi^\dagger \phi) - \lambda_1 [\text{Tr}(\phi^\dagger \phi)]^2 \\ & - \lambda_2 \text{Tr}(\phi^\dagger \phi)^2 + c[\text{Det}(\phi) + \text{Det}(\phi^\dagger)] \\ & + \text{Tr}[H(\phi + \phi^\dagger)], \end{aligned} \quad (3)$$

with $\phi = T_a \phi_a = T_a(\sigma_a + i\pi_a)$ representing a complex (3×3) -matrix. Explicit chiral symmetry breaking is shown in the last term of Eq. (3), where $H = T_a h_a$ is a (3×3) -matrix with nine external fields h_a . Explicit $U(1)_A$ symmetry is given by 't Hooft determinant term with the anomaly term c . m^2 is the tree-level mass of the fields in the absence of symmetry breaking, λ_1 and λ_2 are the two possible quartic coupling constants.

Under the mean-field approximation [36], the total thermodynamic potential density of the quark-meson

TABLE I. The parameters used in our work from Ref. [36].

$m^2[\text{MeV}^2]$	$h_x[\text{MeV}^3]$	$h_y[\text{MeV}^3]$	λ_1	λ_2	$c[\text{MeV}]$
$(342.252)^2$	$(120.73)^3$	$(336.41)^3$	1.4	46.68	4807.84

model at finite temperature T and quark chemical potential μ_f is given by

$$\Omega(T, \mu_f) = \Omega_{q\bar{q}}(T, \mu_f) + U(\sigma_x, \sigma_y). \quad (4)$$

The first term $\Omega_{q\bar{q}}$ in the right hand of Eq. (4) denotes the fermionic part of the thermodynamic potential [36]:

$$\Omega_{q\bar{q}}(T, \mu_f) = 2N_c \sum_{f=u,d,s} T \int \frac{d^3\mathbf{p}}{(2\pi)^3} [\ln(1 - f_{q,f}^0(T, \mu_f, \mathbf{p})) + \ln(1 - f_{\bar{q},f}^0(T, \mu_f, \mathbf{p}))], \quad (5)$$

with the isotropic equilibrium distribution function of (antiquark) quark for f -th flavor

$$f_{q(\bar{q}),f}^0(T, \mu_f, \mathbf{p}) = \frac{1}{\exp[E_f \mp \mu_f/T] + 1}. \quad (6)$$

Here, $E_f = \sqrt{p^2 + m_f^2}$ is the single-particle energy with flavor-dependent constituent quark mass m_f . The sign \mp corresponds to quarks and antiquarks, respectively. In present work, an uniform quark chemical potential $\mu \equiv \mu_u \equiv \mu_d \equiv \mu_s$ is assumed. And the breaking of the $SU(2)$ isospin symmetry is not considered, consequently, the up and down quarks have approximately the same masses, i.e., $m_u \approx m_d$. In the quark-meson model, the constituent quark masses are given as

$$m_l = g\sigma_x/2 \quad \text{and} \quad m_s = g\sigma_y/\sqrt{2}, \quad (7)$$

where l denotes light quarks ($l \equiv u, d$). σ_x and σ_y stand for the non-strange and strange chiral condensates, respectively. The Yukawa coupling g is fixed to reproduce a light constituent quark mass of $m_l \approx 300$ MeV. The second term $U(\sigma_x, \sigma_y)$, *viz.*, the purely mesonic potential, is given as [20, 23, 28]

$$U = -h_x\sigma_x - h_y\sigma_y + \frac{m^2(\sigma_x^2 + \sigma_y^2)}{2} - \frac{c\sigma_x^2\sigma_y}{2\sqrt{2}} + \frac{\lambda_1\sigma_x^2\sigma_y^2}{2} + \frac{(2\lambda_1 + \lambda_2)\sigma_x^4}{8} + \frac{(\lambda_1 + \lambda_2)\sigma_y^4}{4}, \quad (8)$$

where the model parameters: m^2 , h_x , h_y , λ_1 , λ_2 and c as reported in Ref. [36], are shown in Table I. Finally, the behaviors of σ_x and σ_y as the functions of temperature and quark chemical potential can be obtained by minimizing the total thermodynamic potential density, i.e.,

$$\left. \frac{\partial \Omega}{\partial \sigma_x} = \frac{\partial \Omega}{\partial \sigma_y} \right|_{\sigma_x=\bar{\sigma}_x, \sigma_y=\bar{\sigma}_y} = 0, \quad (9)$$

with $\sigma_x = \bar{\sigma}_x, \sigma_y = \bar{\sigma}_y$ being the global minimum.

III. THERMODYNAMIC POTENTIAL WITH MOMENTUM ANISOTROPY

Due to the rapid longitudinal expansion of the partonic matter created in the HICs, an anisotropic deformation of the argument of the isotropic (equilibrium) parton distribution functions is generally used to simulate the momentum anisotropy of QGP [76–92]. A special and widely used spherical momentum deformation introduced by Romatschke and Strickland [76], which is characterized by removing and adding particles along a single momentum anisotropy direction, is applied in this paper. Accordingly, the local distribution function of f -th flavor quarks(antiquarks) in an anisotropic system can be obtained from the isotropic (local equilibrium) distribution function by the rescaling of one preferred direction in momentum space, which is given as

$$f_{aniso}^0(T, \mu_f, \mathbf{p}) = \frac{1}{e^{(\sqrt{\mathbf{p}^2 + \xi(\mathbf{p} \cdot \mathbf{n})^2 + m_f^2} \mp \mu_f)/T} + 1}, \quad (10)$$

Here, the anisotropy parameter ξ , presenting the degree of momentum-space anisotropy, generally can be defined as

$$\xi = \frac{\langle \mathbf{p}_T^2 \rangle}{2\langle p_L^2 \rangle} - 1, \quad (11)$$

where p_L and \mathbf{p}_T are the components of momentum parallel and perpendicular to the direction of anisotropy, \mathbf{n} , respectively. And $\mathbf{p} = (p \sin \theta \cos \phi, p \sin \theta \sin \phi, p \cos \theta)$, where we use a notation $|\mathbf{p}| \equiv p$ for convenience. $\mathbf{n} = (\sin \alpha, 0, \cos \alpha)$, α is the angle between \mathbf{p} and \mathbf{n} . Accordingly, $(\mathbf{p} \cdot \mathbf{n})^2 = p^2(\sin \theta \cos \phi \sin \alpha + \cos \theta \cos \alpha)^2 = p^2 c(\theta, \phi, \alpha)$. Note that $\xi > 0$ corresponds to a contraction of the particle distribution in the direction of anisotropy whereas $-1 < \xi < 0$ stands for a stretching of the particle distribution in the direction of anisotropy.

If the system is close to the ideal massless parton gas and ξ is small, ξ is also related to the ratio of shear viscosity to entropy density η/s as well as the proper time τ of the medium. The relation for one-dimensional Bjorken expansion in the Navier-Stokes limit is given as [94]

$$\xi = \frac{10}{T\tau} \frac{\eta}{s}. \quad (12)$$

This implies that non-vanishing shear viscosity combined with finite momentum relaxation rate in an expanding system can also contribute to the momentum-space anisotropy. At the RHIC energy with the critical temperature $T_c \approx 160$ MeV, $\tau \approx 6$ fm/c and $\eta/s = 1/4\pi$, we can obtain $\xi \approx 0.3$.

In this work, we assume the system has a small deviation from the momentum-space isotropy, therefore

TABLE II. The chiral critical temperature of the non-strange condensate T_c^x and strange condensate T_s^x at vanishing quark chemical potential for different anisotropy parameters.

ξ	-0.4	0	0.2	0.4
$T_c^x(\text{MeV})$	137	146	152	159
$T_s^x(\text{MeV})$	233	248	258	270

the value of ξ is small ($|\xi| \ll 1$) and the Eq. (10) can be expanded up to linear order in ξ ,

$$\begin{aligned} f_{aniso}^0(\mathbf{p}) &\approx f_{q,f}^0 - \frac{\xi(\mathbf{p} \cdot \mathbf{n})^2}{2E_f T} e^{(E_f - \mu_f)/T} f_{q,f}^{02} \\ &= f_{q,f}^0 - \frac{\xi(\mathbf{p} \cdot \mathbf{n})^2}{2E_f T} f_{q,f}^0 (1 - f_{q,f}^0). \end{aligned} \quad (13)$$

By replacing the isotropic distribution functions in Eq. (5) with the Eq. (13), we finally obtain the ξ -dependent thermodynamic potential density of fermionic part

$$\begin{aligned} \Omega_{q\bar{q}} &= 2N_c \sum_f \int \frac{T d^3\mathbf{p}}{(2\pi)^3} \\ &\left\{ \ln(1 - f_{q,f}^0 + \frac{\xi p^2 c(\theta, \phi, \alpha)}{2E_f T} f_{q,f}^0 (1 - f_{q,f}^0)) \right. \\ &\quad \left. + \ln(1 - f_{\bar{q},f}^0 + \frac{\xi p^2 c(\theta, \phi, \alpha)}{2E_f T} f_{\bar{q},f}^0 (1 - f_{\bar{q},f}^0)) \right\}. \end{aligned} \quad (14)$$

Similar to the studies regarding finite-size effect [42] and non-extensive effect [58], we also treat the anisotropy parameter ξ as a thermodynamic argument in the same footing as T and μ , and do not have any modifications to the usual quark-meson model parameters due to the presence of momentum anisotropy. Replacing the fermionic thermodynamic potential in Eq. (9) with Eq. (14), we can finally obtain the ξ -dependent chiral condensates at finite temperature and quark chemical potential.

IV. RESULTS AND DISCUSSIONS

A. phase transition and phase diagram

In the 2+1 flavor quark-meson model, the chiral condensates of both light quarks and strange quarks can be regarded as the order parameters to analyze the feature of the chiral phase transition. The anisotropy parameters we work here are artificially taken as $\xi = -0.4, 0, 0.2, 0.4$, although the value of ξ in the realistic HICs always remains positive in sign. In Fig. 1, the temperature T dependences of non-strange chiral condensate σ_x and strange chiral condensate σ_y for

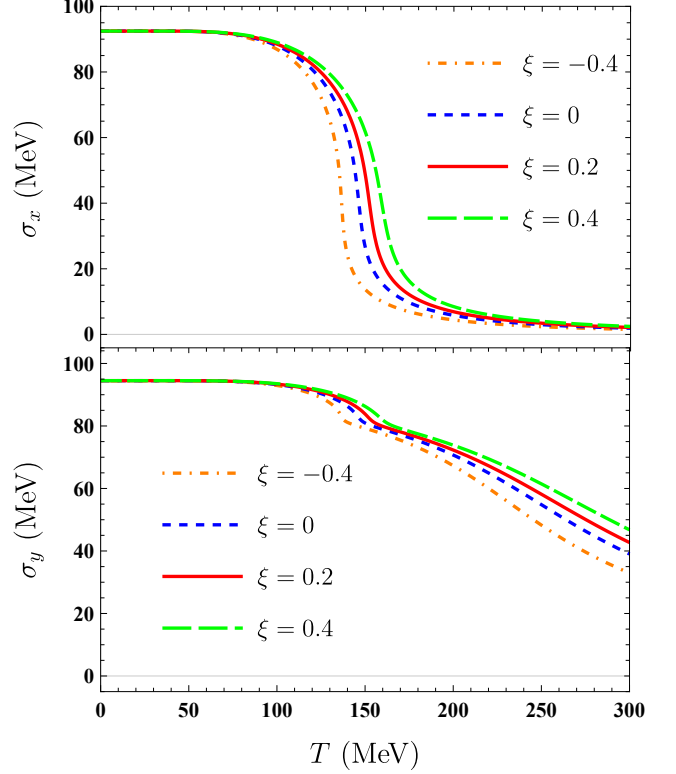


FIG. 1. The temperature dependences of non-strange chiral condensate σ_x (upper panel) and strange chiral condensate σ_y (lower panel) at vanishing quark chemical potential for both isotropic ($\xi = 0$ (blue dashed lines)) and anisotropic (i.e., $\xi = -0.4$ (orange dotted-dashed lines), 0.2 (red solid lines) and 0.4 (green wide dashed lines)) quark matter in quark-meson model. The values of σ_x and σ_y in the vacuum approximately are 92.4 MeV and 94.5 MeV, respectively.

both isotropic and anisotropic quark matter at vanishing quark chemical potential are plotted. For $T = 0$ MeV, $\sigma_x^0 \approx 92.4$ MeV and $\sigma_y^0 \approx 94.5$ MeV. As can be seen, σ_x and σ_y in both isotropic and anisotropic quark matter decrease continuously with increasing temperature. This means that at vanishing quark chemical potential, the restoration of the chiral symmetry for (an-)isotropic quark matter is always a crossover phase transition. And the restoration of the chiral symmetry in the strange sector is always slower than that in the non-strange sector. As ξ increases, the values of σ_x and σ_y increase and their melting behaviors become more smoother. This shows that an increase of anisotropy parameter tends to delay the chiral symmetry restoration.

In order to obtain the chiral critical temperature, we introduce the susceptibilities of light quarks χ_l and strange quarks χ_s , which are defined as

$$\chi_l = -\frac{\partial \sigma_x}{\partial T}, \quad \chi_s = -\frac{\partial \sigma_y}{\partial T}. \quad (15)$$

The thermal behaviors of both χ_l and χ_s are presented in Fig. 2. We can see that χ_l and χ_s are peaking up

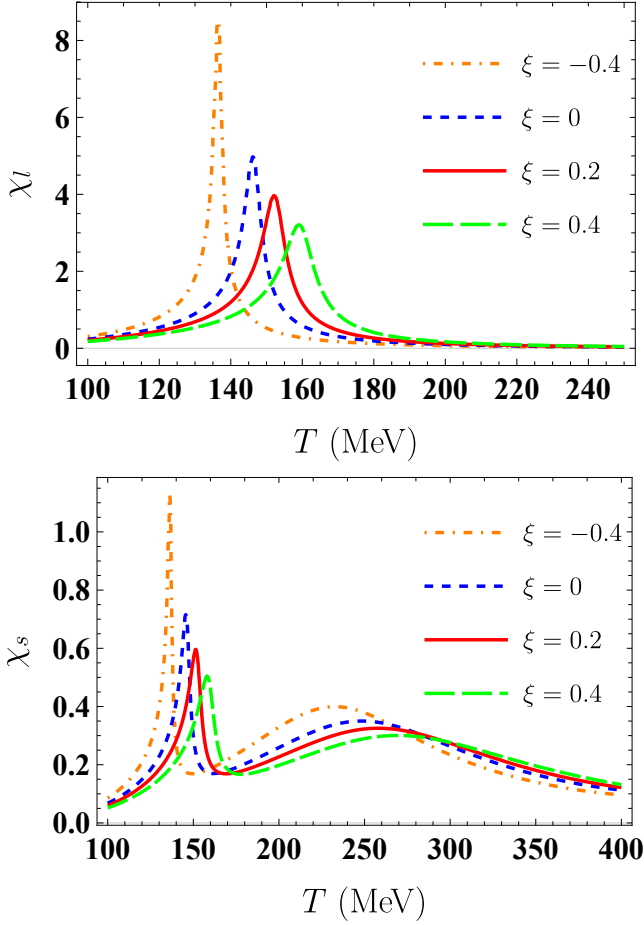


FIG. 2. The temperature dependences of the susceptibilities in non-strange sector χ_l (upper panel) and in strange sector χ_s (lower panel) at $\mu = 0$ GeV for both isotropic ($\xi = 0$ (blue dashed line)) and anisotropic (i.e., $\xi = -0.4$ (orange dotted-dashed line), 0.2 (red solid line)) and 0.4 (green wide dashed line) quark matter in the quark-meson model.

at the particular temperatures. The peak position of χ_l determines the critical temperature T_c^x for the chiral transition in non-strange sector. Different to χ_l , χ_s have two peaks in the entire temperature domain of interest. The temperature coordinate of the first peak of χ_s is almost same as that of χ_l , the location of the second broad peak of χ_s determines the critical temperature for the chiral transition of strange sector T_s^x . The chiral critical temperature T_c^x at vanishing quark chemical potential is the origin of the crossover phase transition in the QCD chiral phase diagram. Furthermore, these chiral critical temperatures are sensitive to the variation of ξ . As ξ increases, $T_{c,s}^x$ shifts towards higher temperatures as well as the height of $\chi_{l,s}$ decreases. The exact values of both T_c^x and T_s^x for different anisotropy parameters are listed in Table II. Compared to the case of $\xi = 0$, the chiral critical temperatures T_c^x and T_s^x decrease by approximately 6% for the case of $\xi = -0.4$. For the cases of $\xi = 0.2$ and 0.4, both T_c^x and T_s^x increase by

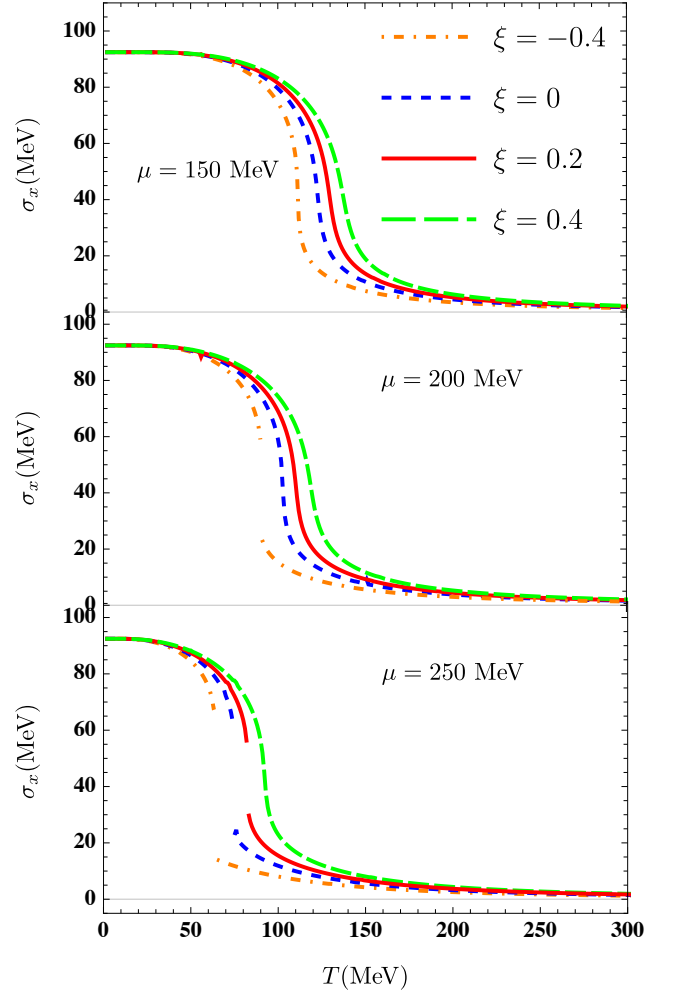


FIG. 3. The temperature dependence of the non-strange chiral condensate at $\mu = 150$ MeV (upper panel), $\mu = 200$ MeV (middle panel) and $\mu = 250$ MeV (lower panel) in quark matter with different anisotropy parameters, i.e., $\xi = -0.4$ (orange dotted-dashed lines), 0.0 (blue dash lines), 0.2 (red solid lines) and 0.4 (green wide dashed lines)

approximately 4% and 9%, respectively.

Next, we extend our exploration to finite quark chemical potential for analyzing the effect of momentum anisotropy on the structure of QCD phase diagram. In Fig. 3, the temperature dependence of non-strange chiral condensate σ_x for both isotropic and anisotropic quark matter at different quark chemical potentials (*viz.*, $\mu = 150$ MeV, 200 MeV, 250 MeV) is plotted. At $\mu = 150$ MeV, the chiral symmetry restoration with different ξ still takes place as the crossover phase transition. For $\mu = 200$ MeV, the value of σ_x in the anisotropic quark matter with $\xi = -0.4$ drops from 60 MeV to 23 MeV, and associated susceptibility presents a divergent behavior at $T = 90$ MeV, which signals the appearance of a first-order phase transition. For $\mu = 250$ MeV, the discontinuity of σ_x (i.e., the first-order phase transition) also occurs at $\xi = -0.4$, 0 and 0.2, whereas, at $\xi = 0.4$

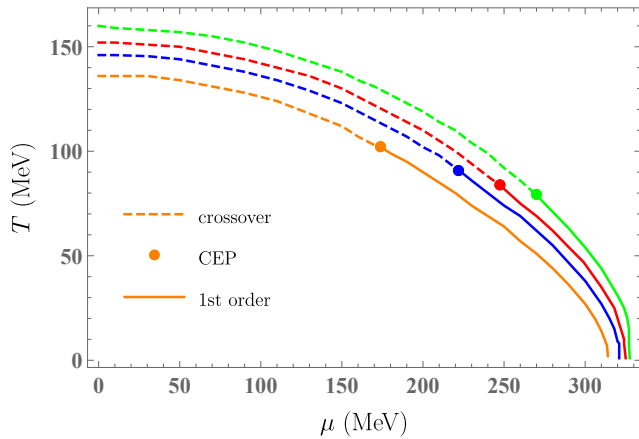


FIG. 4. Chiral phase diagram for different anisotropy parameters in the quark-meson model. The solid lines represent the first-order phase transition curves, the dashed lines denote the crossover transition curves, and the solid dots represent the positions of the CEP (μ_{CEP} , T_{CEP}).

the phase transition is still a smooth crossover. Thus, for the anisotropic matter with $\xi = 0.4$, a first-order phase transition happens at higher quark chemical potential. Accordingly, the chiral phase transition diagram can be studied by outlining the location of T_c^χ for a wide range of quark chemical potential. And the first-order phase transition has to end and then changes into a crossover is the QCD critical endpoint (CEP), at which the phase transition is of second order. In Fig. 4, the 2+1 flavor chiral phase diagram in the (μ, T) -plane for the quark-meson model within the effect of momentum-space anisotropy is presented. Along the first-order phase transition line (crossover phase transition line), the chiral critical temperature rises from zero up to the CEP temperature (from the T_{CEP} up to the $T_c^\chi(\mu = 0)$), whereas the critical quark chemical potential decreases from the $\mu_c(T = 0)$ to the μ_{CEP} (from the μ_{CEP} to zero). We observe that the phase boundary in the (μ, T) -plane of the quark-meson model phase diagram is shifted to higher values of μ and T , with increasing anisotropy parameter. We also can clearly see that the position of the CEP significantly depends on the variation of momentum anisotropy parameter. As ξ increases, the location of the CEP shifts to higher μ and smaller T domain, which is similar to the study of non-extensive effect in linear sigma model [59]. Similar phenomenon is also observed in the literature for analyzing the finite size effects on chiral phase transition [51–54, 57]. In Ref. [51], when the system size is reduced to 4 fm, the CEP in the quark-meson model vanishes and the whole chiral phase boundary becomes a crossover curve. Based on this result, we deduce that as ξ increases further, the CEP may disappear. In this work, for $\xi = -0.4, 0, 0.2, 0.4$, the location of the CEP is at $(T_{CEP}, \mu_{CEP}) = (100, 174)$ MeV, $(91, 222)$ MeV, $(84, 247)$ MeV and

$(79, 270)$ MeV, respectively. The value of μ_{CEP} from $\xi = -0.4$ to $\xi = 0.4$ increases by about 50%, whereas the value of T_{CEP} increases by about 20%. This means that the influence of momentum-space anisotropy on the quark chemical potential coordinate of the CEP is more prominent compared to that on the temperature of the CEP. An opposite trend can be found in the study of finite volume effect [51], where the temperature coordinate of the CEP in the quark-meson model appears to be affected more strongly by the finite volume than CEP's quark chemical potential coordinate.

B. QCD thermodynamic quantities

Let us now study the influence of anisotropy parameter ξ on the thermodynamics at vanishing quark chemical potential. The T - and ξ -dependent pressure $P(T, \xi)$, which is derived from the thermodynamic potential, can be given as

$$P(T, \xi) = -\Omega(T, \xi), \quad (16)$$

with the vacuum normalization $P(0, \xi) = 0$. The entropy density s and energy density ϵ are defined as

$$s(T, \xi) = -\frac{\partial \Omega(T, \xi)}{\partial T} \quad (17)$$

and

$$\epsilon(T, \xi) = -P(T, \xi) + Ts(T, \xi), \quad (18)$$

respectively.

In Fig. 5, the variations of the scaled pressure P/T^4 , scaled entropy density s/T^3 , and scaled energy density ϵ/T^4 with respect to temperature in the quark-meson model for both isotropic and anisotropic quark matter are presented. As can be seen that the thermal behaviors of P/T^4 , s/T^3 , and ϵ/T^4 for the anisotropic quark matter is in agreement with those for the isotropic system. To be specific, with increasing temperature, P/T^4 , s/T^3 , and ϵ/T^4 first rise rapidly then tend towards a saturation value. At high enough temperature, the limit values of P/T^4 , s/T^3 , and ϵ/T^4 in the case of $\xi = -0.4$ stabilize approximately at 4.0, 16.5, 12.5, respectively, although all these values are lower than their respective QCD Stefan-Boltzmann (SB) limit values: $\frac{P_{SB}}{T^4} = (N_c^2 - 1)\frac{\pi^2}{45} + N_c N_f \frac{2\pi^2}{180} \simeq 5.2$, $\frac{s_{SB}}{T^3} = \frac{4P_{SB}}{T^4} \simeq 20.8$, $\frac{\epsilon_{SB}}{T^4} = \frac{3P_{SB}}{T^4} \simeq 15.6$. From Fig. 5 we also can see that the limit values of these thermodynamics at high enough temperature still are decreasing functions of ξ , which is opposite to their qualitative behaviors with the non-extensive parameter q . In Ref. [58], at high temperature, the limit values of these scaled thermodynamics increase as q increases. Moreover, their features with ξ are significantly different to those with finite volume effect. For example, Refs. [43, 54] have indicated that with increasing temperature, P/T^4 first decreases with increasing volume and then quickly saturates to the infinite volume value, in other

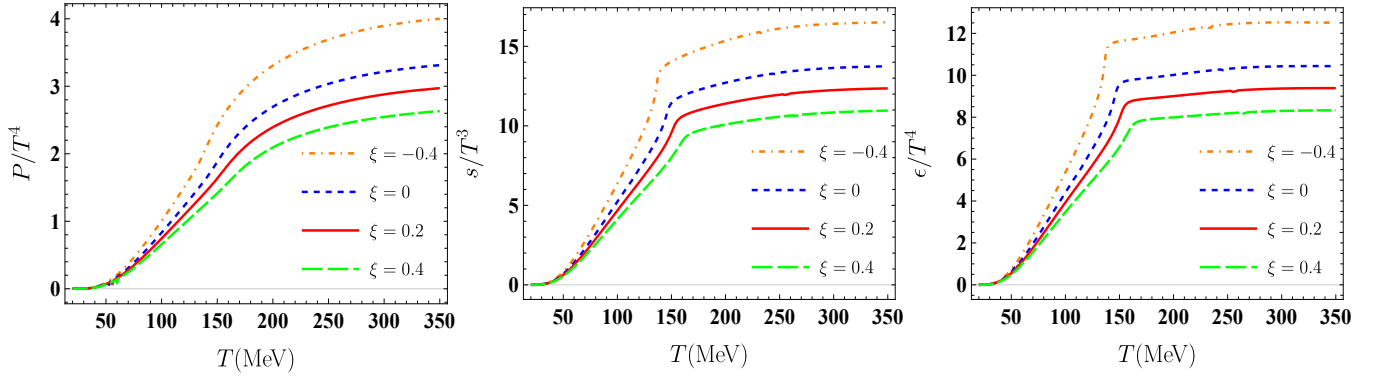


FIG. 5. The temperature dependences of the scaled pressure P/T^4 (left panel), scaled entropy density s/T^3 (middle panel), and scaled energy density ϵ/T^4 (right panel) for $\mu = 0$ MeV in quark matter with different anisotropy parameters, i.e., $\xi = -0.4$ (orange dotted-dashed lines), 0 (blue dash lines), 0.2 (red solid lines) and 0.4 (green wide dashed lines).

word, these thermodynamics are insensitive to volume changes in high temperature domain.

The speed of sound squared c_s^2 as an important quantity in the HICs is also studied in present work. It is defined by

$$c_s^2(T, \xi) = \frac{\partial P}{\partial \epsilon} \Big|_V = \frac{\partial P}{\partial T} \Big|_V \Big/ \frac{\partial \epsilon}{\partial T} \Big|_V = \frac{s}{C_V}, \quad (19)$$

with the specific heat at constant volume V

$$C_V(T, \xi) = \frac{\partial \epsilon}{\partial T} \Big|_V = -T \frac{\partial^2 \Omega}{\partial T^2} \Big|_V. \quad (20)$$

As shown in the upper panel of Fig. 6, the scaled specific heat C_V/T^3 first rises rapidly with increasing temperature, reaches the maximum near the chiral critical temperature T_c^x , then decreases and eventually remains constant. Similar to P/T^4 , s/T^3 , and ϵ/T^4 , the limit value of C_V/T^3 at high temperature also decreases as ξ increases. The peak of C_V/T^3 decreases as ξ increases, in other word, as ξ increases, the critical behavior of C_V/T^3 is smoothed out. From the lower panel of Fig. 6 we see that the thermal behavior of the speed of sound squared c_s^2 for $\xi = -0.4$ exhibits a sharp drop near the corresponding chiral critical temperature T_c^x , then increases rapidly up to the ideal gas value of $1/3$. Moreover, as ξ increases, the dip structure of c_s^2 is gradually weakened and the location of its minimum shifts to higher temperatures, which is qualitatively similar to C_V/T^3 . At high temperature, we can see that c_s^2 is nearly unaffected by ξ , which is due to that the reduction in entropy density and the increment in inverse specific heat almost cancel each other out. The literature for the studies of finite-size effect [42, 43] and non-extensive effect [58] in PNJL model also has indicated

that as the system size L (non-extensive parameter q) decreases (increases), the critical behavior of c_s^2 gradually dilutes and even vanishes. Therefore, these results of thermodynamics again emphasize that the increase of ξ can hinder the restoration of chiral symmetry.

C. Meson mass

In this part, we study the chiral structures of scalar ($J^P = 0^+$) and pseudoscalar ($J^P = 0^-$) meson masses at vanishing quark chemical potential. A detailed procedure for calculating meson masses at finite temperature and quark chemical potential in the quark-meson model can be found in Ref. [36]. Here, we just sketch the outline of the related computation. In quantum field theory, the scalar and pseudoscalar meson masses generally can be obtained from the second derivative of the temperature- and quark chemical potential-dependent thermodynamic potential density $\Omega(T, \mu_f)$ with respect to corresponding the scalar fields $\alpha_{S,a} = \sigma_a$ and the pseudoscalar fields $\alpha_{P,a} = \pi_a$ ($a = 0, \dots, 8$), which can be expressed as [36]

$$m_{i,ab}^2 = \frac{\partial^2 \Omega(T, \mu_f)}{\partial \alpha_{i,a} \partial \alpha_{i,b}} \Big|_{\min} = (m_{i,ab}^M)^2 + (m_{i,ab}^T)^2 \quad (21)$$

where the subscript $i = S(P)$ denotes the scalar (pseudoscalar) mesons. The first term on the right-hand side of Eq. (21) is vacuum mass squared matrices calculated from the second derivative of purely mesonic potential. The second term represents the modification of mass squared matrices due to fermionic thermal correction at finite temperature and quark chemical potential, which in an anisotropic system can be written as

$$\begin{aligned}
(\delta m_{i,ab}^T)^2 &= \frac{\partial \Omega_{q\bar{q}}(T, \mu_f, \xi)}{\partial \alpha_{i,a} \partial \alpha_{i,b}} \\
&= 2N_c \sum_{f=l,s} \int \frac{dp}{4\pi^2} \frac{p^2}{E_f} \left\{ \left[f_{q,f}^0 \left(m_{f,ab}^2 - \frac{m_{f,a}^2 m_{f,b}^2}{2E_f^2} \right) - \frac{f_{q,f}^0 (1 - f_{q,f}^0)}{2E_f T} m_{f,a}^2 m_{f,b}^2 \right] \right. \\
&\quad \times \left[1 - \frac{\xi p^2}{6E_f T} (1 - f_{q,f}^0 + \frac{T}{E_f}) \right] + \frac{\xi p^2 f_{q,f}^0}{12E_f^2 T^2} m_{f,a}^2 m_{f,b}^2 \left[\frac{2T^2}{E_f^2} + \frac{T}{E_f} - \frac{T f_{q,f}^0}{E_f} - f_{q,f}^0 (1 - f_{q,f}^0) \right] + q \rightarrow \bar{q} \Bigg\}. \quad (22)
\end{aligned}$$

The squared constituent quark mass derivative with respect to meson field $\partial m_f^2 / \partial \alpha_{i,a} \equiv m_{f,a}^2$, and that with respect to meson fields $\partial^2 m_f^2 / (\partial \alpha_{i,a} \partial \alpha_{i,b}) \equiv m_{f,ab}^2$ for different flavors are listed in the Table III of Ref. [36]. When $\xi = 0$, Eq. (22) can reduce to the result for an isotropic system. Thereafter, the squared masses of four scalar meson states are given as [23, 36, 37]

$$m_{a_0}^2 = (m_{a_0}^M)^2 + (\delta m_{S,11}^T)^2, \quad (23)$$

$$m_{\kappa}^2 = (m_{\kappa}^M)^2 + (\delta m_{S,44}^T)^2, \quad (24)$$

$$m_{\sigma}^2 = m_{S,00}^2 \cos^2 \theta_S + m_{S,88}^2 \sin^2 \theta_S + 2m_{S,08}^2 \sin \theta_S \cos \theta_S, \quad (25)$$

$$m_{f_0}^2 = m_{S,00}^2 \sin^2 \theta_S + m_{S,88}^2 \cos^2 \theta_S - 2m_{S,08}^2 \sin \theta_S \cos \theta_S. \quad (26)$$

And the four pseudoscalar meson masses are

$$m_{\pi}^2 = (m_{\pi}^M)^2 + (\delta m_{P,11}^T)^2, \quad (27)$$

$$m_K^2 = (m_K^M)^2 + (\delta m_{P,44}^T)^2, \quad (28)$$

$$m_{\eta'}^2 = m_{P,00}^2 \cos^2 \theta_P + m_{P,88}^2 \sin^2 \theta_P + 2m_{P,08}^2 \sin \theta_P \cos \theta_P, \quad (29)$$

$$m_{\eta}^2 = m_{P,00}^2 \sin^2 \theta_P + m_{P,88}^2 \cos^2 \theta_P - 2m_{P,08}^2 \sin \theta_P \cos \theta_P, \quad (30)$$

where the mixing angles $\theta_{S(P)}$ read as

$$\tan 2\theta_i = \left(\frac{2m_{i,08}^2}{m_{i,00}^2 - m_{i,88}^2} \right), \quad i = S, P. \quad (31)$$

and $m_{i,00/88/08}^2 = (m_{i,00/88/08}^M)^2 + \delta(m_{i,00/88/08}^T)^2$. The detailed descriptions of the vacuum contributions $[(m_{a_0}^M)^2, (m_{\kappa}^M)^2, (m_{\pi}^M)^2, (m_K^M)^2 \text{ and } (m_{i,00/88/08}^M)^2]$ from purely mesonic potential in Eqs. (23)-(30) can be found from Refs. [36, 37].

The left panels and right panels of Fig. 7 display the T -dependent masses of the pseudoscalar (π , K , η' , η) and scalar (f_0 , σ , a_0 , κ) mesons for both isotropic and anisotropic quark matter in the quark-meson model, respectively. We can see that for a fixed anisotropy parameter, the masses of the pseudoscalar meson sectors π , K , and η remain constant up to near the chiral critical temperature of non-strange condensate T_c^x , whereas the masses of η' and scalar meson sectors σ , a_0 , κ remain

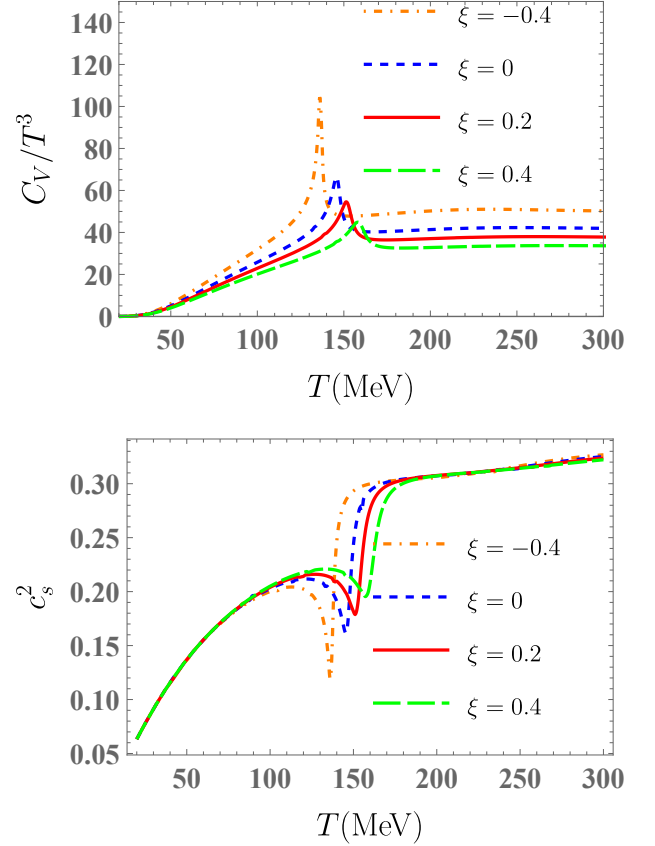


FIG. 6. The temperature dependences of the scaled specific heat C_V/T^3 (upper panel) and the squared speed of sound c_s^2 (lower panel) at $\mu = 0$ MeV for isotropic ($\xi = 0$ (blue dashed lines)) and anisotropic (i.e., $\xi = -0.4$ (orange dotted-dashed lines), 0.2 (red solid lines) and 0.4 (green wide dashed lines) quark matter in the quark-meson model.

constant at low temperature and then decreases before reaching T_c^x . For the pseudoscalar meson sector f_0 , its mass also remains constant at low temperature but decreases before reaching the chiral critical temperature of strange condensate T_s^x . For pseudoscalar meson sectors π , K and η , their masses always decrease with increasing ξ at $T > 140$ MeV. However, for η' and pseudoscalar meson sectors (π , K , η' , η), the dependence of their masses on anisotropy parameter ξ is nonmonotonic in the entire temperature domain of

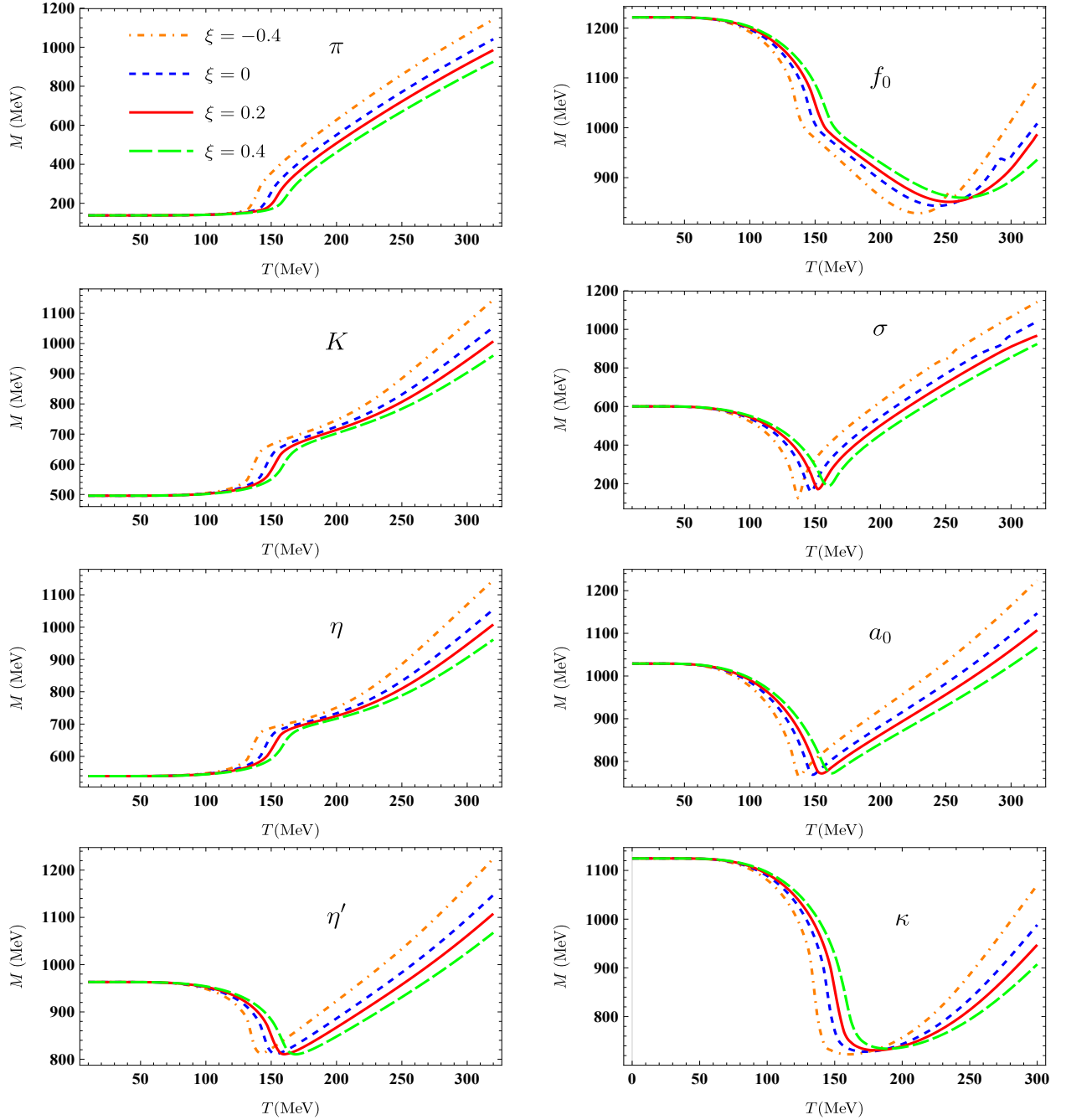


FIG. 7. The temperature dependences of the pseudoscalar mesons π , K , η' , η (left panels) and scalar mesons f_0 , σ , a_0 , κ (right panels) at $\mu = 0$ MeV for both isotropic ($\xi = 0$ (blue dashed lines)) and anisotropic (i.e., $\xi = -0.4$ (orange dotted-dashed lines), 0.2 (red solid lines) and 0.4 (green wide dashed lines) quark matter in the quark-meson model.

interest. More exact, with the increase of ξ , the masses of η' , σ , a_0 , κ first increase in low temperature domain ($100 \text{ MeV} < T < 160 \text{ MeV}$), then decrease in higher temperature domain ($T > 160 \text{ MeV}$). For f_0 , its mass increases with increasing ξ at $T < 270 \text{ MeV}$ (viz., $T_s^x(\xi = 0.4)$) and decreases afterward. As a whole, near above T_c^x or T_s^x , all mesons become unphysical degrees of freedom and their masses become degenerate, which signals the

restoration of chiral symmetry. In Fig. 7 we can also see that with the increase of ξ , the temperature coordinate at which meson masses begin to degenerate can be shifted to higher temperatures. This again shows that an increase of momentum-space anisotropy parameter can hinder the restoration of chiral symmetry. The qualitative behaviors of these meson masses with ξ are different to the results for analyzing the finite size dependence of meson masses

within PNJL model [43, 47], where K , η , and η' have a significant volume dependence in lower temperature domain ($T < 100$ MeV).

D. Transport coefficient

Studying transport properties is essential to deeply understand the dynamical evolution of the strongly interacting matter. In this part, we discuss the influence

of momentum-space anisotropy on transport coefficients, such as shear viscosity η , electrical conductivity σ_{el} , and bulk viscosity ζ in quark matter. Due to the effect of momentum-space anisotropy is encoded in the parton distribution functions, the general expressions of these transport coefficients, which are obtained by solving the relativistic Boltzmann equation in relaxation time approximation, need to do some modifications [89–92]. Therefore, using the results in Refs. [90, 91], the formulas of ξ -dependent transport coefficients at zero quark chemical potential are given as

$$\eta = \sum_f \frac{d_f}{15T} \int \frac{dp}{\pi^2} \frac{p^6}{E_f^2} [\tau_{q,f} f_{q,f}^0 (1 - f_{q,f}^0)] - \sum_f \frac{\xi d_f}{90T^2} \int \frac{dp}{\pi^2} \frac{p^8}{E_f^3} [\tau_{q,f} f_{q,f}^0 (1 - f_{q,f}^0) (1 - 2f_{q,f}^0 + \frac{T}{E_f})], \quad (32)$$

$$\sigma_{el} = \sum_f \frac{d_f q_f^2}{3T} \int \frac{dp}{\pi^2} \frac{p^4}{E_f^2} [\tau_{q,f} f_{q,f}^0 (1 - f_{q,f}^0)] (1 + \frac{\xi}{3}) - \sum_f \frac{q_f^2 \xi d_f}{18T^2} \int \frac{dp}{(2\pi)^3} \frac{p^6}{E_f^3} [f_{q,f}^0 (1 + f_{q,f}^0) (1 - 2f_{q,f}^0 + \frac{T}{E_f})], \quad (33)$$

$$\begin{aligned} \zeta = & \sum_f \frac{d_f}{T} \int \frac{dp}{\pi^2} \frac{p^2}{E_f} \left[\left(\frac{1}{3} - c_s^2 \right) p^2 - c_s^2 m_f^2 + c_s^2 m_f T \frac{dm_f}{dT} \right]^2 [\tau_{q,f} f_{q,f}^0 (1 - f_{q,f}^0)] \\ & - \sum_f \frac{\xi d_f}{6T^2} \int \frac{dp}{\pi^2} \frac{p^4}{E_f^3} \left[\left(\frac{1}{3} - c_s^2 \right) p^2 - c_s^2 m_f^2 + c_s^2 m_f T \frac{dm_f}{dT} \right]^2 [\tau_{q,f} f_{q,f}^0 (1 - f_{q,f}^0) (1 - 2f_{q,f}^0)] \\ & - \sum_f \frac{\xi d_f}{6T} \int \frac{dp}{\pi^2} \frac{p^4}{E_f^4} \left[\frac{1}{9} p^4 - \left(c_s^2 (m_f^2 + p^2) - c_s^2 m_f T \frac{dm_f}{dT} \right)^2 \right] \tau_{q,f} f_{q,f}^0 (1 - f_{q,f}^0). \end{aligned} \quad (34)$$

Here, d_f is the degeneracy factor for f -flavor quark. The quark electric charge q_f is given explicitly by $q_u = -q_{\bar{u}} = 2e/3$ and $q_{d,s} = -q_{\bar{d},\bar{s}} = -e/3$. The electron charge reads $e = (4\pi\alpha_s)^{1/2}$ with the fine structure constant $\alpha_s \simeq 1/137$. Different to the formula of bulk viscosity in Ref. [91], we replace the original term $[(\frac{1}{3} - c_s^2)p^2]^2$ in the integrand with $[(\frac{1}{3} - c_s^2)p^2 - c_s^2 m_f^2 + c_s^2 m_f T \frac{dm_f}{dT}]^2$ to incorporate the in-medium effect. In the treatment of the relaxation time $\tau_{q,f}$, we roughly take a constant value $\tau_{q,f} = 1$ fm for the computation. In the weakly anisotropic system, the former terms in Eqs. (32)-(34) are significantly larger than the latter terms in magnitude due to the difference in momentum power of respective integrand. Therefore, transport coefficients are still mainly dominated by the first term of related expressions on the quantitative.

The variation of shear viscosity η with temperature at vanishing quark chemical potential for both isotropic and anisotropic quark matter is shown in Fig. 8. We see that η in the (an)-isotropic quark matter rises monotonically with increasing temperature because the T dependence of η is mainly coming from the quark distribution function $f_{q,f}^0$ in the associated integrand. For the qualitative behavior of η with ξ , we also can well understand

from the associated expression. In the vicinity of the chiral critical temperature T_c^X , η slightly decreases as ξ grows due to decreasing behavior of the Boltzmann factor $e^{-m_f(T)/T}$ with ξ . In higher temperature domain ($T > 160$ MeV), the decreasing feature of η is negligible due to the unsensitivity of the constituent quark masses to ξ . However, the absolute value of the second term in Eq. (32) significantly increases with an increase of ξ . As a result, η decreases as ξ grows. This is similar to the result in Ref. [91], where η for the QGP is calculated in quasiparticle model. For electrical conductivity σ_{el} , its thermal behavior is similar to η , the quantitative difference between η and σ_{el} is mainly coming from the different momentum power of respective integrand. Similar to shear viscosity, the ξ dependence of σ_{el} is also determined by the second term in the associated expression. In Fig. 9, we observe that σ_{el} decreases as ξ increases, which is also qualitatively consistent with the results of σ_{el} for the QGP in quasiparticle model [89, 92]. The dependences of η and σ_{el} on momentum-space anisotropy are different from those on finite system size L in the framework of (P)NJL model. In Ref. [42], both η and σ_{el} first increase as L decreases in low temperature domain, whereas, the size effect nearly vanishes in high temperature domain. Furthermore, the result in Ref. [58]

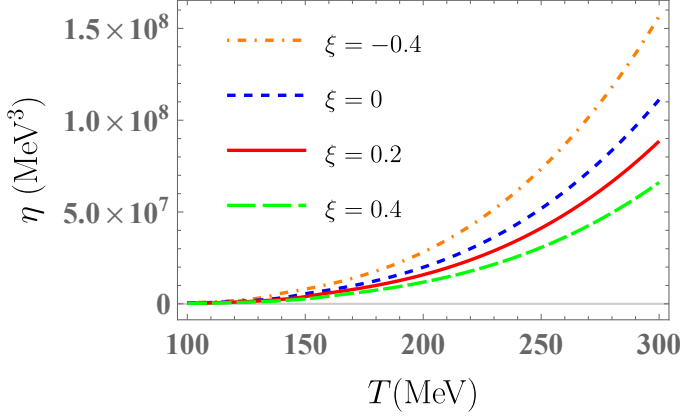


FIG. 8. The temperature dependence of shear viscosity η at $\mu = 0$ MeV in quark matter with $\xi = -0.4$ (orange dotted-dashed line), 0.0 (blue dashed line), 0.2 (red solid line), 0.4 (green wide dashed line).

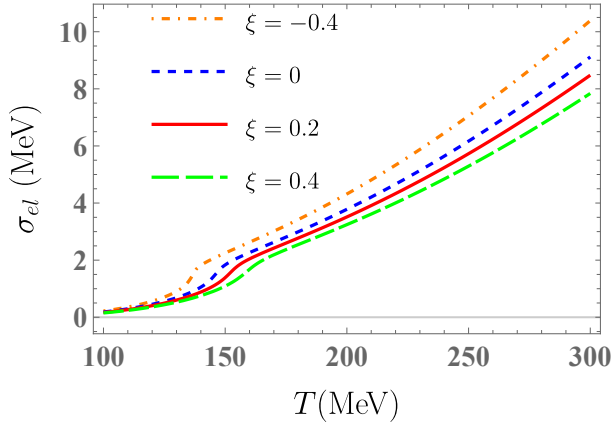


FIG. 9. The temperature dependence of electrical conductivity σ_{el} at $\mu = 0$ MeV in quark matter with $\xi = -0.4$ (orange dotted-dashed line), 0.0 (blue dashed line), 0.2 (red solid line), 0.4 (green wide dashed line).

has indicated that both η and σ_{el} in PNJL model also increase obviously as non-extensive parameter q increases at $T > 150$ MeV.

Next, we discuss the temperature dependence of bulk viscosity ζ at zero quark chemical potential for both isotropic and anisotropic quark matter. As shown in Fig. 10, for a fixed anisotropy parameter, ζ is peaking up in the vicinities of both T_c^χ and T_s^χ , which is significantly different to the thermal behaviors of η and σ_{el} . We also note that the thermal profile of ζ is similar to dm_s/dT or χ_s , which may be attributed that the qualitative behavior of ζ is mainly govern by dm_s/dT rather than the quark distribution function in associated integrand of Eq. (34). Due to the decreasing feature of the peak of dm_s/dT with increasing ξ , the double-peak structure of ζ can be weakened as ξ grows and the positions of peaks shift to higher temperatures, as shown in Fig. 10. The

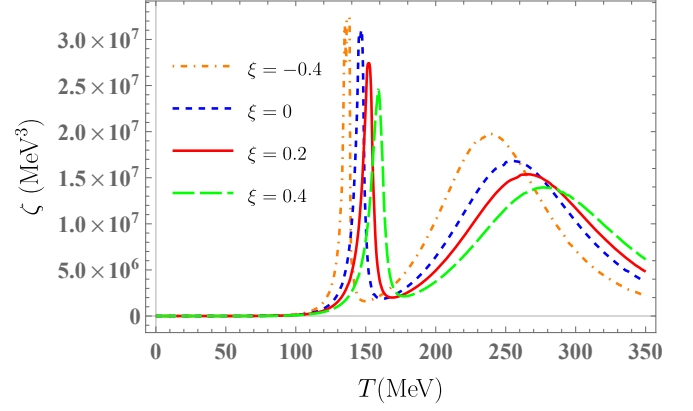


FIG. 10. The temperature dependence of bulk viscosity ζ at $\mu = 0$ MeV in quark matter with $\xi = -0.4$ (orange dotted-dashed line), 0.0 (blue dashed line), 0.2 (red solid line), 0.4 (green wide dashed line).

diluting effect of ξ on the critical behavior of ζ is similar to the studies regarding finite volume effect and non-extensive effect. In Ref. [42], the double-peak structure of ζ even converts to one broadened peak structure when the system size is reduced to 2 fm. And in Ref. [58], as non-extensive parameter q increases to 1.1, the two peaks of ζ also begin to merge into a broad one.

V. SUMMARY AND CONCLUSION

In this work, an anisotropy parameter ξ , which reflects the degree of momentum-space anisotropy arising from different expansion rates of the fireball generated in HICs along longitudinal and radial direction, for the first time, is introduced in the 2+1 flavor quark-meson model by replacing the isotropic distribution function in the thermodynamic potential of the quark-meson model with the anisotropic one. The effect of ξ on the chiral properties, thermodynamics, meson masses, and transport properties in quark matter are investigated. We find that the chiral phase transition of quark matter with different anisotropy parameters is always a crossover at vanishing quark chemical potential. At finite quark chemical potential, the temperature of the CEP is affected more significantly by the anisotropy parameter than its quark chemical potential, which is opposite to the study of finite volume effect. We also demonstrate that at high temperature, the limit values of various scaled thermodynamics (P/T^4 , s/T^3 , ϵ/T^4 , C_V/T^3) are quite sensitive to ξ . As ξ increases, their limit values decrease, which is different to the finite size effect but rather similar to non-extensive effect. And the critical behavior of C_V/T^3 and c_s^2 can be smoothed out with increasing ξ . For scalar and pseudoscalar mesons, the

temperature, where their masses begin to degenerate, is enhanced as ξ rises, which implies that an increase of ξ can hinder the restoration of chiral symmetry. Finally, the transport coefficients, such as shear viscosity η , electrical conductivity σ_{el} , and bulk viscosity ζ for both isotropic and anisotropic quark matter, are also calculated. Our results show that η and σ_{el} rise with increasing temperature, while the thermal behavior of ζ exhibits a noticeable double-peak structure. It is seen that η and σ_{el} decrease monotonically as ξ increases, whereas the qualitative behavior of ζ with ξ is similar to $\chi_s(\xi)$. With increasing ξ , the double-peak structure of ζ can be weakened, and the positions of peaks shift to higher temperatures.

In present work, we only focus on the chiral aspect of the QCD phase diagram, the exploration of the confinement phase transition in an anisotropic quark matter also can be addressed via including the Polyakov-loop potential. In the Polyakov-loop improved quark-meson model, the chiral phase transition and the location of the CEP will be affected further. For the calculation of transport coefficients in this study, the relaxation

time of quark is assumed to be a constant. However, in the realistic interaction scenario, the relaxation time may also vary with the momentum anisotropy. These issues are our future research directions. Moreover, note that a spheroidal momentum-space anisotropy specified by one anisotropy parameter in one preferred propagation direction is considered in this work, however, the introduction of additional anisotropy parameters is necessary to provide a better characterization of the QGP properties. The chiral and confinement phase transitions in quark matter with ellipsoidal momentum-anisotropy [78, 79] characterized by two independent anisotropy parameters, also can be done using PNJL or PQM model. The works of these directions are in progress and we expect to report our results soon.

ACKNOWLEDGMENTS

This work is supported by the National Natural Science Foundation of China under Grants No.11935007.

-
- [1] C. Bernard *et al.* [MILC Collaboration], Phys. Rev. D **71**, 034504 (2005).
 - [2] Y. Aoki, G. Endrodi, Z. Fodor, S. D. Katz, and K. K. Szabo, Nature **443**, 675 (2006).
 - [3] K. Splittorff and J. J. M. Verbaarschot, Phys. Rev. D **75**, 116003 (2007).
 - [4] K. Fukushima and C. Sasaki, Prog. Part. Nucl. Phys. **72**, 99 (2013).
 - [5] K. Fukushima and T. Hatsuda, Rept. Prog. Phys. **74**, 014001 (2011).
 - [6] P. Braun-Munzinger, V. Koch, T. Schäfer and J. Stachel, Phys. Rept. **621**, 76 (2016).
 - [7] C. R. Allton, M. Doring, S. Ejiri, S. J. Hands, O. Kaczmarek, F. Karsch, E. Laermann and K. Redlich, Phys. Rev. D **71**, 054508 (2005).
 - [8] R. V. Gavai and S. Gupta, Phys. Rev. D **78**, 114503 (2008).
 - [9] R. V. Gavai and S. Gupta, Phys. Rev. D **68**, 034506 (2003).
 - [10] Z. Fodor and S. D. Katz, JHEP **0203**, 014 (2002).
 - [11] Z. Fodor, S. D. Katz and K. K. Szabo, Phys. Lett. B **568**, 73 (2003).
 - [12] J. R. Klauder, Phys. Rev. A **29**, 2036 (1984).
 - [13] G. Aarts, E. Seiler and I. O. Stamatescu, Phys. Rev. D **81**, 054508 (2010).
 - [14] Y. Nambu and G. Jona-Lasinio, Phys. Rev. **124**, 246 (1961).
 - [15] T. Hatsuda and T. Kunihiro, Phys. Rept. **247**, 221 (1994).
 - [16] S. P. Klevansky, Rev. Mod. Phys. **64**, 649 (1992).
 - [17] P. N. Meisinger and M. C. Ogilvie, Phys. Lett. B **379**, 163 (1996).
 - [18] S. Roessner, C. Ratti and W. Weise, Phys. Rev. D **75**, 034007 (2007).
 - [19] C. Ratti, S. Roessner and W. Weise, Phys. Lett. B **649**, 57 (2007).
 - [20] B. J. Schaefer and J. Wambach, Nucl. Phys. A **757**, 479 (2005).
 - [21] B. J. Schaefer, J. M. Pawłowski and J. Wambach, Phys. Rev. D **76**, 074023 (2007).
 - [22] B. J. Schaefer and J. Wambach, Phys. Rev. D **75**, 085015 (2007).
 - [23] J. T. Lenaghan, D. H. Rischke and J. Schaffner-Bielich, Phys. Rev. D **62**, 085008 (2000).
 - [24] J. Schaffner-Bielich, Phys. Rev. Lett. **84**, 3261 (2000).
 - [25] B. J. Schaefer, M. Wagner and J. Wambach, Phys. Rev. D **81**, 074013 (2010).
 - [26] U. S. Gupta and V. K. Tiwari, Phys. Rev. D **81**, 054019 (2010).
 - [27] R. Stiele and J. Schaffner-Bielich, Phys. Rev. D **93**, no. 9, 094014 (2016).
 - [28] B. J. Schaefer and M. Wagner, Phys. Rev. D **85**, 034027 (2012).
 - [29] C. S. Fischer, Prog. Part. Nucl. Phys. **105**, 1 (2019).
 - [30] A. Bashir, L. Chang, I. C. Cloet, B. El-Bennich, Y. X. Liu, C. D. Roberts and P. C. Tandy, Commun. Theor. Phys. **58**, 79 (2012).
 - [31] J. M. Pawłowski, Annals Phys. **322**, 2831 (2007).
 - [32] C. Bagnuls and C. Bervillier, Phys. Rept. **348**, 91 (2001).
 - [33] B. J. Schaefer and J. Wambach, Phys. Part. Nucl. **39**, 1025 (2008).
 - [34] H. Gies, Lect. Notes Phys. **852**, 287 (2012).
 - [35] U. S. Gupta and V. K. Tiwari, Phys. Rev. D **85**, 014010 (2012).
 - [36] B. J. Schaefer and M. Wagner, Phys. Rev. D **79**, 014018 (2009).
 - [37] A. N. Tawfik and A. M. Diab, Phys. Rev. C **91**, no. 1, 015204 (2015).

- [38] A. Abhishek, H. Mishra and S. Ghosh, *Phys. Rev. D* **97**, no. 1, 014005 (2018).
- [39] S. Ghosh, F. E. Serna, A. Abhishek, G. Krein and H. Mishra, *Phys. Rev. D* **99**, no. 1, 014004 (2019).
- [40] P. Singha, A. Abhishek, G. Kadam, S. Ghosh and H. Mishra, *J. Phys. G* **46**, no. 1, 015201 (2019).
- [41] A. Bzdak, S. Esumi, V. Koch, J. Liao, M. Stephanov and N. Xu, *Phys. Rept.* **853**, 1 (2020).
- [42] K. Saha, S. Ghosh, S. Upadhyaya and S. Maity, *Phys. Rev. D* **97**, no. 11, 116020 (2018).
- [43] A. Bhattacharyya, P. Deb, S. K. Ghosh, R. Ray and S. Sur, *Phys. Rev. D* **87**, no. 5, 054009 (2013).
- [44] Z. Zhang, C. Shi and H. Zong, *Phys. Rev. D* **101**, no. 4, 043006 (2020).
- [45] J. Braun, B. Klein and P. Piasecki, *Eur. Phys. J. C* **71**, 1576 (2011).
- [46] N. Magdy, *Universe* **5**, no. 4, 94 (2019).
- [47] Y. P. Zhao, P. L. Yin, Z. H. Yu and H. S. Zong, *Nucl. Phys. B* **952**, 114919 (2020).
- [48] P. Deb, S. Ghosh, J. Prakash, S. K. Das and R. Varma, *arXiv:2005.12037 [nucl-th]*.
- [49] L. M. Abreu, E. B. S. Corrêa, C. A. Linhares and A. P. C. Malbouisson, *Phys. Rev. D* **99**, no. 7, 076001 (2019).
- [50] C. Shi, Y. Xia, W. Jia and H. Zong, *Sci. China Phys. Mech. Astron.* **61**, no. 8, 082021 (2018).
- [51] R. A. Tripolt, J. Braun, B. Klein and B. J. Schaefer, *Phys. Rev. D* **90**, no. 5, 054012 (2014).
- [52] B. L. Li, Z. F. Cui, B. W. Zhou, S. An, L. P. Zhang and H. S. Zong, *Nucl. Phys. B* **938**, 298 (2019).
- [53] L. F. Palhares, E. S. Fraga and T. Kodama, *J. Phys. G* **38**, 085101 (2011).
- [54] N. Magdy, M. Csanád and R. A. Lacey, *J. Phys. G* **44** (2017) no.2, 025101.
- [55] J. Braun, B. Klein and B. J. Schaefer, *Phys. Lett. B* **713**, 216 (2012).
- [56] J. Braun, B. Klein, H.-J. Pirner and A. H. Rezaeian, *Phys. Rev. D* **73**, 074010 (2006).
- [57] Y. P. Zhao, R. R. Zhang, H. Zhang and H. S. Zong, *Chin. Phys. C* **43**, no. 6, 063101 (2019).
- [58] Y. P. Zhao, *Phys. Rev. D* **101**, no. 9, 096006 (2020).
- [59] K. M. Shen, H. Zhang, D. F. Hou, B. W. Zhang and E. K. Wang, *Adv. High Energy Phys.* **2017**, 4135329 (2017).
- [60] J. O. Andersen, W. R. Naylor and A. Tranberg, *Rev. Mod. Phys.* **88**, 025001 (2016).
- [61] K. Fukushima, M. Ruggieri and R. Gatto, *Phys. Rev. D* **81**, 114031 (2010).
- [62] R. Gatto and M. Ruggieri, *Phys. Rev. D* **83**, 034016 (2011).
- [63] M. Ruggieri, M. Tachibana and V. Greco, *JHEP* **1307**, 165 (2013).
- [64] K. Kashiwa, *Phys. Rev. D* **83**, 117901 (2011).
- [65] J. O. Andersen, W. R. Naylor and A. Tranberg, *JHEP* **1502**, 042 (2015).
- [66] J. O. Andersen, W. R. Naylor and A. Tranberg, *JHEP* **1404**, 187 (2014).
- [67] L. Yu, J. Van Doorselaere and M. Huang, *Phys. Rev. D* **91**, no. 7, 074011 (2015).
- [68] S. Mao, *Phys. Lett. B* **758**, 195 (2016).
- [69] S. Ghosh, B. Chatterjee, P. Mohanty, A. Mukharjee and H. Mishra, *Phys. Rev. D* **100**, no. 3, 034024 (2019).
- [70] A. N. Tawfik and N. Magdy, *Phys. Rev. C* **91**, 015206 (2015).
- [71] W. R. Tavares and S. S. Avancini, *Phys. Rev. D* **97**, no. 9, 094001 (2018).
- [72] M. Ruggieri, Z. Y. Lu and G. X. Peng, *Phys. Rev. D* **94**, no. 11, 116003 (2016).
- [73] G. Cao and X. G. Huang, *Phys. Rev. D* **93**, no. 1, 016007 (2016).
- [74] M. Ruggieri and G. X. Peng, *Phys. Rev. D* **93**, no. 9, 094021 (2016).
- [75] W. R. Tavares, R. L. S. Farias and S. S. Avancini, *Phys. Rev. D* **101**, no. 1, 016017 (2020).
- [76] P. Romatschke and M. Strickland, *Phys. Rev. D* **68**, 036004 (2003); *Phys. Rev. D* **70**, 116006 (2004).
- [77] B. Schenke and M. Strickland, *Phys. Rev. D* **74**, 065004 (2006).
- [78] B. S. Kasmaei, M. Nopoush and M. Strickland, *Phys. Rev. D* **94**, no. 12, 125001 (2016).
- [79] B. S. Kasmaei and M. Strickland, *Phys. Rev. D* **97**, no. 5, 054022 (2018).
- [80] L. Bhattacharya, R. Ryblewski and M. Strickland, *Phys. Rev. D* **93**, no. 6, 065005 (2016).
- [81] B. S. Kasmaei and M. Strickland, *arXiv:1911.03370 [hep-ph]*.
- [82] B. Schenke and M. Strickland, *Phys. Rev. D* **76**, 025023 (2007).
- [83] B. S. Kasmaei and M. Strickland, *Phys. Rev. D* **99**, no. 3, 034015 (2019).
- [84] M. Y. Jamal, I. Nilima, V. Chandra and V. K. Agotiya, *Phys. Rev. D* **97**, no. 9, 094033 (2018).
- [85] Y. Burnier, M. Laine and M. Vepsäläinen, *Phys. Lett. B* **678**, 86 (2009).
- [86] L. Thakur, N. Haque, U. Kakade and B. K. Patra, *Phys. Rev. D* **88**, no. 5, 054022 (2013).
- [87] M. Nopoush, Y. Guo and M. Strickland, *JHEP* **1709**, 063 (2017).
- [88] A. Dumitru, Y. Guo and M. Strickland, *Phys. Lett. B* **662**, 37 (2008).
- [89] L. Thakur, P. K. Srivastava, G. P. Kadam, M. George and H. Mishra, *Phys. Rev. D* **95**, no. 9, 096009 (2017).
- [90] H. X. Zhang, *arXiv:2004.08767 [hep-ph]*.
- [91] S. Rath and B. K. Patra, *Phys. Rev. D* **100**, no. 1, 016009 (2019); *arXiv:2001.11788 [hep-ph]*.
- [92] P. K. Srivastava, L. Thakur and B. K. Patra, *Phys. Rev. C* **91**, no. 4, 044903 (2015).
- [93] D. Giataganas, *JHEP* **1207**, 031 (2012).
- [94] M. Asakawa, S. A. Bass and B. Muller, *Prog. Theor. Phys.* **116**, 725 (2007).